Bi-velocity gas dynamics of a micro lid-driven cavity heat transfer subject to forced-convection

Bi-velocity gas dynamics of a micro lid-driven cavity heat transfer subject to forced-convection

S Kokou Dadzie* and Chariton Christou

School of Engineering and Physical Sciences

Heriot-Watt University, Edinburgh,

EH14 4AS, Scotland, UK

Abstract:

We investigate heat transfer in a rarefied gas in a lid-driven cavity flow initiated by instantaneously heating and cooling opposite walls for different flow regimes. Volume diffusion model is used as an extension to the standard Navier-Stokes-Fourier set for simulating the flows. Numerical simulations are presented and compared with standard Navier-Stokes-Fourier. For higher Knudsen numbers the volume diffusion model captures non-local equilibrium effects in corners of the cavity that are missed by the Navier-Stokes-Fourier model. It is generally observed that one can use volume diffusion corrections to capture disequilibrium effects in high rarefaction regimes.

1. Introduction

Lid-driven cavity flow problem is often used to benchmark new continuum fluid models as several investigations are carried out using the configuration [1, 2]. The various heat transfer mechanics, namely, natural convection, forced-convection and mixed-convection are all investigated using hydrodynamic models as understanding thermal behaviors of a lid-driven cavity fuels applications in electronic cooling, manufacturing processes and others. Iwatsu and Hyun provided a numerical study of three dimensional flows in a cubical container with stable vertical temperature stratification [3]. Ghasemi and Aminossadati presented the numerical study of mixed-convection in a lid-driven filled with water and nanoparticles [4] . Cheng and Liu investigated the effect of the cavity inclination on mixed convection heat transfer [5].

With advances in nano- and micro-electromechnical systems (NEMS/MEMS) in fabrication technology, understanding new mass and heat transfer processes in rarefaction regimes is of another great interest. Accurate modelling of gas flows at micro/nano scale involves in principle accurate modelling of rarefaction, gas-surface interactions and inter-molecular collisions [6]. To determine the degree of gas rarefaction, the Knudsen number (Kn) is introduced, $Kn = \lambda/L$ where λ is the mean free path of the gas molecules and L is a characteristic length of the flow system [7]. Existing models in dealing with these transport phenomena include continuum, molecular and hybrid methods. The standard continuum fluid approach is thought to be valid for $Kn \leq 0.001$. It may be extended beyond $Kn = 0.01$ into the slip-flow regime by introducing velocity slip and temperature jump at boundaries. For $0.01 \leq Kn \leq 10$, in the transition regime, the continuum assumption breaks down and Boltzmann equation and other particle methods are adopted. The flow is considered as a free-molecular flow for $Kn > 10$ where intermolecular collisions become rare. Gas flows in MEMS and NEMS are usually in the slip ($Kn \leq 0.01$) and transition regimes ($0.01 \leq Kn \leq 10$).

Heat transfer characteristics in rarefied gas in the driven cavity problem are in paucity in the

Corresponding author: *k.dadzie@hw.ac.uk

literature. Mizzi *et al.* provided DSMC flow features in the cavity in the slip flow regime [8]. General agreement is reported between NSF and DSMC at Kn=0.02 and 0.05 in the velocity fields and differences for the temperature fields. Though understanding counter-gradients heat transfer mechanism exhibited in the DSMC flow contours are still indistinct and are not predictable by NSF. Boundary treatment is determinant in DSMC flow feature predictions[9]. The inappropriateness of the standard NSF model in describing temperature field in a stationary gas in the continuum limit has long been shown by Sone *et al.* [10]. These authors therefore provided corrections to the standard constitutive equations involving Korteweg diffuse interface type stress tensor required to acquire appropriate heat transfer description in a gas around a body at rest in a close domain.

An alternative continuum approach to the description of a fluid accounting for its non-continuum aspect has been recently introduced [11]. This theory was first initiated based on the observation in thermophoresis experiments [12]. The underlying principle is the existence of two independent velocities in any continuum fluid; the volume velocity and the mass velocity [13]. The resulting equations are completed in a thermo-mechanically consistent continuum flow equations[14]. A numerical analysis using this approach to predict gas dynamics in a micro-channel Couette flow is presented in [15]. It was concluded that the Bi-velocity (volume diffusion) equations show reasonable results compared with existing Burnett equations that are traditionally derived from the Boltzmann equation. An analytical solution based on this new continuum approach to the prediction of gas mass flow rates in a pressure driven rarefied gas over a range of Knudsen numbers is presented in [16]. It was found that volume diffusion (Bi-velocity) theory concords with experimental data from low to Knudsen number of 5.

In the present paper we propose an additional lid-driven cavity flow configuration to evaluate heat transfer mechanics in non-equilibrium rarefaction regimes. We compare volume diffusion continuum approach with standard NSF. It is generally observed that the volume diffusion continuum approach may allow for better description of counter-gradient heat transfer mechanics.

2. The Mixed-Convection Problem

Sketch of the problem under investigation and boundary conditions are shown in Figure 1. It is a two-dimensional square cavity of length $W = 50\mu m$ and aspect ratio of one. The cavity is filled with compressible monoatomic argon, *Ar*, with negligible gravity force. The horizontal walls are adiabatic with the top moving at velocity $\boldsymbol{U_w}$ = 100 m/s generating a forced convection. The left vertical wall is kept at the lower temperature (T_c = 273K) and the right vertical wall at the higher temperature (T_H = 283K). Various different cases of Knudsen numbers are considered ranging from 0.001 to 10. The mean free path (λ) is calculated using,

$$\lambda = \frac{2(5-2\omega)(7-2\omega)}{15}\left(\frac{m}{2\pi kT}\right)^{\frac{1}{2}}\left(\frac{\mu}{\rho}\right) \qquad 2.1$$

with ω the temperature coefficient, m the atomic mass, and k the Boltzmann constant, μ the dynamic viscosity, T the temperature and ρ the mass-density of the gas [17]. Configuration in

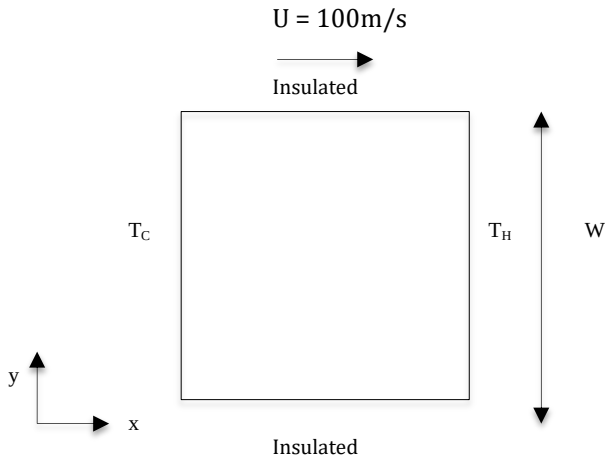

Figure 1. Problem Configuration

3. The continuum fluid model with volume diffusion correction

Starting with a modified particle probability distribution function and associated Boltzmann-like kinetic equation, a new set of Burnett-regime continuum model was derived in [14]. The principle of the volume diffusion theory is the inclusion of an additional transport term originating from the gas molecular level spatial distribution. It was shown that this description leads to a set of Burnett-regime continuum model that, in contrast with all existing Burnett regime models based on the original Boltzmann equation, is consistent with all known mechanical and thermodynamic principles. A set of transport equations were given as:

$$\mathrm{D}\rho = -\rho\nabla\cdot\boldsymbol{U_m} \tag{3.1a}$$

$$\bar{\rho}\mathrm{D}\left(ln\frac{\bar{\rho}}{\rho}\right) = -\frac{\bar{\rho}}{p}\nabla\cdot[p\boldsymbol{J_c}] \tag{3.1b}$$

$$\rho\mathrm{D}\boldsymbol{U_m} = -\nabla\cdot[\boldsymbol{P_v} - \rho\boldsymbol{J_c}\boldsymbol{J_c}] \tag{3.1c}$$

$$\rho T\mathrm{D}\bar{s} = -\nabla\cdot[\boldsymbol{q_{ve}}] - \boldsymbol{\Pi_v} : \nabla[\boldsymbol{U_m} - \boldsymbol{J_c}] \tag{3.1d}$$

where $\boldsymbol{U_m}$ is the mass velocity, ρ is a mass-density following definition of the gas molecular probability density distribution, $\bar{\rho}$ is the reciprocal of the gas specific volume and differs initially from ρ due to the principle of volume diffusion. The pressure tensor is $\boldsymbol{P_v}$, p is the pressure, T is the temperature and $\boldsymbol{\Pi_v} = \boldsymbol{P_v} - p\mathbf{I}$ represents the shear stress tensor. The material derivative is defined as,

$$\mathrm{D} = \frac{\partial}{\partial t} + \boldsymbol{U_m}\cdot\nabla \tag{3.2}$$

In the set of equations (3.1) $\boldsymbol{q_{ve}}$ is the entropic heat flux given by the Fourier's law [14] :

$$\boldsymbol{q_{ve}} = \boldsymbol{q_v} + \rho e_{in}\boldsymbol{J_c} = -k\nabla T \tag{3.3}$$

where k is the thermal conductivity. The specific internal energy of the fluid is $e_{in} = (3/2)\,RT$. We note in the above equations the appearance of the new term $\boldsymbol{J_c}$. Flux $\boldsymbol{J_c}$ is the

molecular level diffusive flux of gas molecule concentration. In other words $-\boldsymbol{J_c}$ represents a gas volume diffusive flux. It characterizes macroscopically, the difference between the fluid volume velocity $\boldsymbol{U}_v$ and the fluid mass velocity $\boldsymbol{U_m}$ [18]:

$$\boldsymbol{J_c} = -\boldsymbol{U_v} + \boldsymbol{U_m} = -\frac{k_m}{\rho}\nabla\rho \tag{3.4}$$

where k_m is the molecular diffusivity coefficient. This coefficient may be related to the dynamic viscosity, μ, as:

$$k_m \equiv \frac{\mu}{\rho} \tag{3.5}$$

In this volume diffusion continuum description, mass conservation is described in the separate equation (3.1.a) while equation (3.1.b) originated from a non-conservative transport equation for the gas volume accounting for its dynamics. In order to achieve a full thermodynamic consistency the specific entropy $\bar{s}$ is defined through:

$$\rho T \boldsymbol{D}\bar{s} = \bar{\rho} p \boldsymbol{D}\bar{\rho}^{-1} + \rho \boldsymbol{D}\left[e_{in} - \frac{1}{2}\boldsymbol{J_c}^2\right] \tag{3.6}$$

This modified Gibbs equation together with the volume transport equation and the energy equation allow satisfying the second law of thermodynamics. Shear stress $\boldsymbol{\Pi_v}$ is then based upon the fluid volume velocity:

$$\boldsymbol{\Pi_v} = -2\mu\ \overset{\circ}{\overline{\nabla[\boldsymbol{U_m}\text{-}\boldsymbol{J_c}]}} \tag{3.7}$$

with

$$\overset{\circ}{\overline{\nabla[\boldsymbol{U_m}\text{-}\boldsymbol{J_c}]}} = \frac{1}{2}\left(\nabla\boldsymbol{U_v} + \widetilde{\nabla\boldsymbol{U_v}}\right) - \frac{1}{3}\mathbf{I}\nabla\cdot\boldsymbol{U_v} \tag{3.8}$$

with $\widetilde{\nabla\boldsymbol{U_m}}$ denoting the transpose tensor of $\nabla\boldsymbol{U_m}$ and **I** the identity matrix.

Solution Method using OpenFOAM

The set (3.1) initially developed from four transport equations: mass, volume, gas particle momentum and gas particle kinetic energy. An explicit distinction between a transport equation for the fluid volume and a conservation equation for the mass has been proved important in the description of sound wave dispersion in rarefied gases [19]. In this study focusing on the influence of the volume diffusion flux in the expression of the shear stress and the heat flux, we adopt the simplified conservative form [20]:

Conservation of mass

$$\frac{\partial\rho}{\partial t} + \nabla\cdot[\rho\boldsymbol{U_m}] = 0 \tag{3.9a}$$

Conservation of momentum

$$\frac{\partial\rho\boldsymbol{U_m}}{\partial t} + \nabla\cdot[\rho\boldsymbol{U_m}\boldsymbol{U_m}] + \nabla\cdot[p\boldsymbol{I} + \boldsymbol{\Pi}] = 0 \tag{3.9b}$$

Conservation of total energy

$$\frac{\partial}{\partial t}\left[\frac{1}{2}\rho\boldsymbol{U_m^2} + \rho e_{in}\right] + \nabla\cdot\left[\frac{1}{2}\rho\boldsymbol{U_m^2}\boldsymbol{U_m} + \rho e_{in}\boldsymbol{U_m}\right] + \nabla\cdot[(p\boldsymbol{I} + \boldsymbol{\Pi})\cdot\boldsymbol{U_m}] + \nabla\cdot\boldsymbol{J_u} = 0 \tag{3.9c}$$

where the shear stress term $\boldsymbol{\Pi}$ is given by,

$$\boldsymbol{\Pi} = \boldsymbol{\Pi_v} - \rho \boldsymbol{J_c J_c} \tag{3.10}$$

and the energetic heat flux, $\boldsymbol{J_u}$, is given by,

$$\boldsymbol{J_u} = \boldsymbol{q_{ve}} + p\boldsymbol{J_c} \tag{3.11}$$

In classical NSF theory $\boldsymbol{J_u}$ and $\boldsymbol{q_{ve}}$ are equivalent. Distinction between the energetic heat flux and the entropic heat flux is a fundamental new aspect of the volume diffusion continuum model as energy equation and entropy equations are systematically differentiated. The new energetic heat flux has a component not driven by temperature gradient [11]. The set (3.9) - (3.11) may also be regarded merely as a compressible Korteweg fluid-like set of equations, which is here adopted to evaluate a heat transfer problem in rarefied gas in a micro cavity [21].

To solve the set of equations (3.9) - (3.11) a solver developed in OpenFOAM was considered [22]. The solver is a modification to pre-existing solver called *rhoCentralFoam* [23]. OpenFoam uses finite volume (FV) numeric to solve systems of partial differential equations on three-dimensional unstructured mesh. The solver is a density-based solver and uses a more physical form of the equations described above [23]. Momentum and heat diffusion are introduced to the solver by including the appropriate diffusive terms from equations (3.10) - (3.11). The momentum and energy equations are first solved for $\rho\mathbf{U_m}$ and ρE where E is the total energy density. The solver starts with a solution for the momentum equation:

$$\frac{\partial \dot{\mathbf{U}}}{\partial t} + \nabla \cdot \left[\mathbf{U_m}\dot{\mathbf{U}}\right] + \nabla p = 0 \tag{3.12}$$

where $\dot{\mathbf{U}} = \rho\mathbf{U_m}$. The velocity is then updated by $\mathbf{U_m} = \dot{\mathbf{U}}/\rho$. We then solve a diffusion correction for $\mathbf{U_m}$:

$$\frac{\partial \rho \boldsymbol{U_m}}{\partial t} - \nabla \cdot (\mu \nabla \boldsymbol{U_m}) + \nabla \cdot (\mu \nabla \boldsymbol{J_c}) - \nabla \cdot \left(\boldsymbol{\Pi}_{exp}\right) = 0 \tag{3.13}$$

where the stress tensor component, $\boldsymbol{\Pi}_{exp} = \mu\,[(\nabla\mathbf{U_v})^{\mathrm{T}} - (\frac{2}{3})\mathrm{tr}(\nabla\mathbf{U_v})\mathbf{I}]$ is treated explicitly while the complementary Laplacian term $\nabla \cdot\ (\mu\nabla(\mathbf{U_m} - \mathbf{J_c}))$ is implemented implicitly in $\mathbf{U_m}$ and $\mathbf{J_c}$.

Solving for $\dot{E}$ in the energy equation:

$$\frac{\partial \dot{E}}{\partial t} + \nabla \cdot \left[\mathbf{U_m}\left(\dot{E} + p\right)\right] + \nabla \cdot (\boldsymbol{\Pi} \cdot \mathbf{U_m}) = 0 \tag{3.14}$$

where $\dot{E} = \rho E$. The temperature is updated from ρ, $\mathbf{U_m}$ and $\dot{E}$ using the equation:

$$T = \frac{1}{c_v}\left(\frac{\dot{E}}{\rho} - \frac{|\mathbf{U_m}|^2}{2}\right) \tag{3.15}$$

with E the total energy density:

$$E = e_{in} + \frac{|U_m|^2}{2} \tag{3.16}$$

Then solving for a diffusion correction for T:

$$\left(\frac{\partial(\rho c_v T)}{\partial t}\right) - \nabla \cdot (k\nabla T) - \nabla \cdot \left(k_m \frac{p}{\rho}\nabla\rho\right) = 0 \tag{3.17}$$

The distinction between entropic and energetic heat flux implements some correcting factors, which imply some changes in the transport coefficients. Brenner suggested that equation (3.5) should be multiplied by a dimensionless coefficient (C_{vv}) whose numerical value is near unity [24]:

$$k_m^* = C_{vv}\frac{\mu}{\rho} \tag{3.18}$$

For our solver it was found convenient to set the dimensionless coefficient as, $C_{vv} = \frac{P_r}{3}$, where P_r is the Prandtl number.

The simplified set of volume diffusion equations (3.9) is equivalent to that used in [25]. In that study, Greenshields and Reese reported a numerical overshoot for some values of the volume diffusivity coefficient. Same overshoot problems are observed in our investigations. For example for value of volume diffusivity coefficient where C_{vv} is close to Pr or higher our solutions diverge. In fact, we note that the simplified form of the in equations (3.9) is not a linearly stable set of equations for all values of the volume diffusivity coefficient. Only the full set of equation (3.1) is linearly stable for all value of the volume diffusivity coefficient. The overshoot problem may therefore be resolved by solving the actual set of four initial equations. However, this is beyond the scoop of this paper.

Boundary Conditions

For both methods boundary conditions are implemented in OpenFOAM. For the two continuum methods, NSF and volume diffusion, a temperature jump boundary conditions were imposed [26]:

$$\mathrm{T} - \mathrm{T_w} = -\frac{2-\sigma_\mathrm{T}}{\sigma_\mathrm{T}}\frac{2\gamma}{(\gamma+1)\mathrm{P_r}}\lambda\nabla_\mathbf{n}\mathrm{T} \tag{3.19}$$

$\nabla_\mathbf{n} \equiv \mathbf{n}\cdot\nabla$ is the component of the gradient normal to the boundary surface and $\mathbf{n}$ is the unit normal vector defined as positive in the direction of the flow domain. $\mathrm{T_w}$ is the wall temperature; γ is the specific heat ratio and σ_T the thermal accommodation coefficient. For all our simulations the perfect energy accommodation, σ_T=1, is considered.

Maxwell slip boundary condition was used for NSF on the velocity [27]:

$$\boldsymbol{U_m} - \boldsymbol{U_w} = -\left(\frac{2-\sigma_\mathrm{u}}{\sigma_\mathrm{u}}\right)\frac{\lambda}{\mu}\boldsymbol{\tau} - \frac{3}{4}\frac{\mathrm{Pr}(\gamma-1)}{\gamma\mathrm{p}}\mathbf{q} \tag{3.20}$$

where $\mathbf{U_w}$ is the wall velocity, σ_u is the tangential momentum accommodation coefficient and $\boldsymbol{\tau}$ is the tangential shear stress, $\boldsymbol{\tau} = \mathbf{S}\cdot(\mathbf{n}\cdot\boldsymbol{\Pi}_\mathbf{NSF})$, where the tensor $\mathbf{S} = \mathbf{I} - \mathbf{nn}$ and $\boldsymbol{\Pi}_\mathbf{NSF} = \mu\nabla\mathbf{U_m} + \mu(\nabla\mathbf{U_m})^T - \frac{2}{3}\mathbf{I}\mathrm{tr}(\nabla\mathbf{U_m})$ and $\mathbf{q} = -k\nabla T\cdot\mathbf{S}$

For the volume diffusion continuum model a slip boundary conditions is based on the new shear stress tensor and new heat flux vector as follows:

$$\boldsymbol{U_m} - \boldsymbol{U_w} = -\left(\frac{2-\sigma_\mathrm{u}}{\sigma_\mathrm{u}}\right)\frac{\lambda}{\mu}\boldsymbol{\tau_v} - \frac{3}{4}\frac{\mathrm{Pr}(\gamma-1)}{\gamma\mathrm{p}}\mathbf{j_u} \tag{3.21}$$

where $\boldsymbol{\tau_v}$ is the new tangential shear stress, $\boldsymbol{\tau_v} = \mathbf{S}\cdot(\mathbf{n}\cdot\boldsymbol{\Pi_v})$ and $\mathbf{j_u} = \mathbf{J_u}\cdot\mathbf{S}$. With regards to the volume diffusion set of equations, the new formula (3.21) is the new way of accounting

globally for the importance of boundary effects in the micro and nano regimes without dealing explicitly with a gas/surface interaction model at the molecular level.

For our numerical simulations, in order to find the appropriate number of cells, a grid dependency test was run for 80 x 80, 160 x 160 and 240 x 240 cells. The mesh containing 240 cells in each direction was selected. The courant number, C_r was set to 0.5 for all cases. Three cases for C_r=0.2, C_r=0.4 and C_r=0.5 were tested in order to investigate the dependency of the continuum methods on different time steps. The viscosity for the simulations was $\mu = 1{,}69 \times 10^{-5}$ Pa s. Table 1 presents the flow characteristic numbers including the Reynold number (Re) and Peclet number across the simulation range. These are calculated using the flow average density and average velocity with mass (volume) diffusivity coefficient given by equation (3.18) and the mean free path calculated using equation (2.1) with the flow initial pressure.

Kn	λ(m)	W(m)	Re	Lewis Number	Peclet Number	Mass Transfer Peclet number
0.001	5.0E-08	5.0E-05	296	7	195	1346
0.005	2.5E-07	5.0E-05	290	7	191	1319
0.01	5.0E-07	5.0E-05	258	7	170	1172
0.5	2.5E-05	5.0E-05	66	7	44	302
1	5.0E-05	5.0E-05	40	7	26	182
10	5.0E-04	5.0E-05	4	7	3	20

Table 1: Flow characteristic numbers across the simulation range

4. Results

Figure 2 shows temperature and pressure distributions near the top wall. The top right wall region is the most in non-equilibrium state. At Kn = 0.001 NSF and volume diffusion methods predict the same temperature distribution with the lower temperature on the left wall and the higher on the right. From Kn = 0.005 differences in predictions by the two methods start to appear first in the top right-hand wall region. The difference between the two methods occurs around the pick temperature and becomes noticeable at Kn = 0.01 where though the overall temperature trend remains similar. As we increase the Knudsen number to 1, NSF temperature profile becomes constant; i.e., NSF no longer captures any temperature variation caused by the movement of the top lid. NSF with slip and jump conditions fail completely to capture the disequilibrium in the flow field imposed by the moving lid. Volume diffusion model, however, shows a non-uniform temperature distribution with boundary layers near both walls typical of Knudsen layers. We also observed temperature jumps at both walls. The pressure profiles are normalized with P_0 = 97500Pa and are shown in Figure 2b. The pressure distribution is the same at all Knudsen numbers between the two methods. This means that, with the mixed convection configuration investigated here, no significant correction to the momentum equation is observed. Temperature and heat transfer processes are the most affected by the volume diffusion correction in that configuration. Meanwhile, the equality observed in the temperature profile for Knudsen number less than 0.001 with a deviation above that value confirms that the volume diffusion correction to NSF model is a way of distinguishing between the different flow regimes.

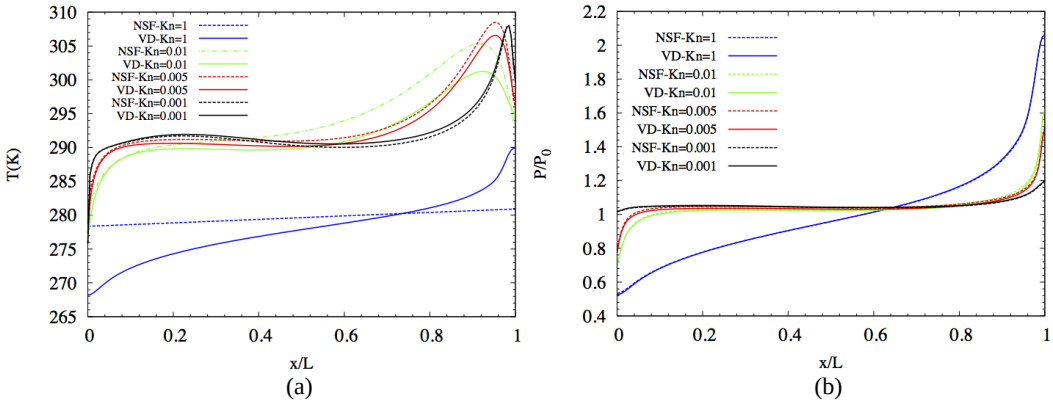

Figure 2: Comparison of the temperature (a) and pressure (b) profiles along the top wall

Figure 3 shows the variation of maximum heat fluxes as a function of Knudsen number in the domain. Highest maximum heat flux is predicted by volume diffusion model. Energetic heat flux is always higher than the entropic heat flux and both are well above heat flux predicted by NSF.

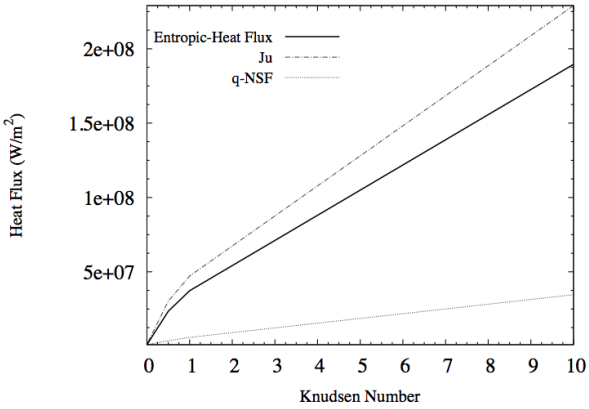

Figure 3: Variation of maximum heat flux with Knudsen number

Figure 4 depict the temperature field at Kn = 0.001 along with the heat flux. Energetic heat flux and entropic heat flux for the volume diffusion model, and classical heat flux from the Navier-Stokes-Fourier are shown. We observe at that Knudsen number the same temperature contours for the three heat fluxes. The left wall is the cooling wall according to the set boundary conditions. The top right corner of the cavity has an increase in temperature due to viscous dissipation and strong non-equilibrium effects. The heat transfer is from hot-to-cold in the entire cavity.

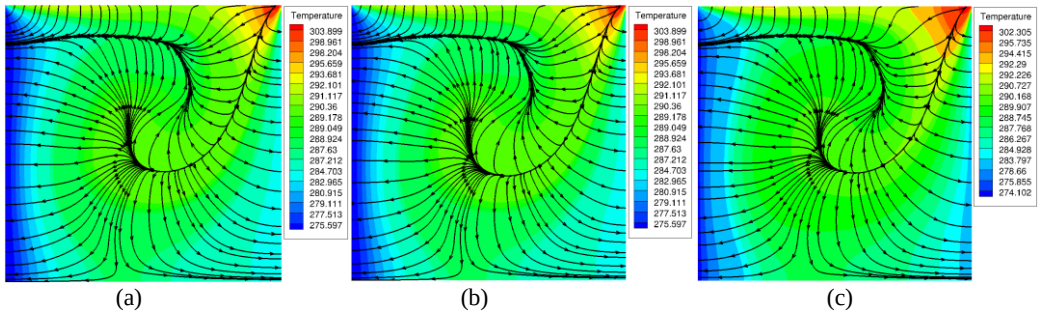

Figure 4: Temperature distribution and heat fluxes at Kn = 0.001 for the (a) energetic heat flux ($\boldsymbol{J_u}$), (b) entropic heat flux ($\boldsymbol{q_{ve}}$) and (c) heat flux for the conventional NSF ($\boldsymbol{q_{NSF}}$)

Contour plots for Knudsen number corresponding to the transition regime (Kn = 0.5) are in Figure 5. Lowest and highest temperatures as predicted by NSF and volume diffusion now differ by about 8 degrees. The temperature drop across the cavity obtained by volume diffusion is higher than that of NSF. The volume diffusion model (Fig 5a,b) shows the two top corners in non-equilibrium state. The lowest temperature occurs in the top left due to expansion cooling. Though, gas molecules leaving that region transport out, generally, higher translational kinetic energy. This is the indication of the direction of the energetic heat flux in Figure 5a in that corner. It is a demonstration of flow phenomena in which temperature is not systematically synonymous with the gas molecule translational kinetic energy. Overall, heat transfers in Figure 5a are the results of combined mass diffusion and forced convection as effects of the disturbing moving lid can be seen along the top wall. Entropic heat flux in Figure 5b shows a flow from the top right corner, i.e. the highest temperature and non-equilibrium region, to cold areas. This is an explicit expression of the second law of thermodynamics corresponding to the configuration. From Figure 5a the higher temperature observed in the top right corner appears as a result of compression of gas molecules coming from the top and right walls at lower translational kinetic energy. Temperature variation predicted by the NSF is in Figure 5c. It simply depicts heat diffusion from higher kinetic energy region on the right, to the lower kinetic energy region on the left. Effects of the moving lid are almost non-existent in the NSF temperature contours. In contrast, in Figure 5a three main phenomena accompanying the energetic heat transfer process in the volume diffusion model may be stated: expansion cooling that takes place in the top left corner, compression in the right corner and the usual heat conduction transfer process.

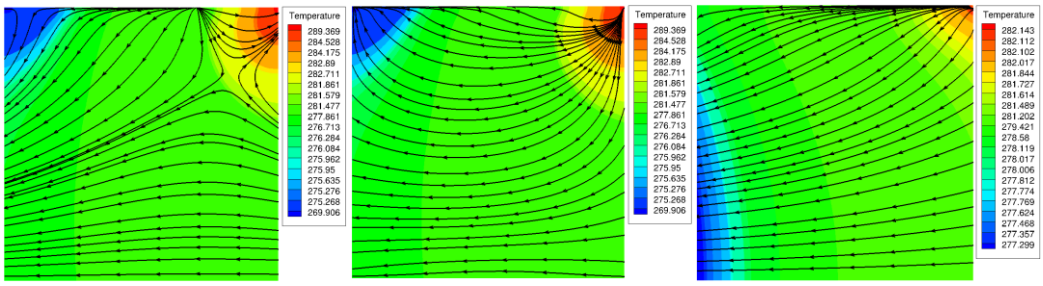

(a) (b) (c)

Figure 5: Temperature distribution and heat fluxes at Kn = 0.5 for the (a) energetic heat flux ($\boldsymbol{J_u}$), (b) entropic heat flux ($\boldsymbol{q_{ve}}$) and (c) heat flux for the conventional NSF ($\boldsymbol{q_{NSF}}$)

Temperature contours in the high transition regime is represented by Figure 6 at Kn=10. Phenomena observed in the early transition regime are now fully developed. NSF displays a constant temperature across the cavity, i.e. none of the disequilibrium conditions is captured by NSF. Energetic heat flux in Figure 6a from the volume diffusion model shows again non-equilibrium state. An unconventional energetic heat transfer from cold-to-hot in the upper left corner as well as in the right corner occurs. The moving top lid induces these non-equilibrium effects. In Figure 6b, entropy flows from top right corner into the top left corner which is again consistent with the second law.

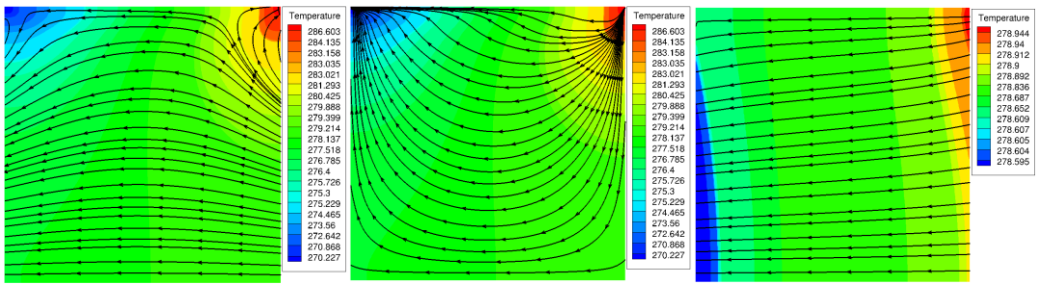

(a) (b) (c)

Figure 6: Temperature distribution and heat fluxes at Kn = 10 for the (a) energetic heat flux ($\boldsymbol{J_u}$), (b) entropic heat flux ($\boldsymbol{q_{ve}}$) and (c) heat flux for the conventional NSF ($\boldsymbol{q_{NSF}}$)

Generally, volume diffusion process in the present forced convection configuration appears physically as a counter-diffusion process. That is, a process where molecules with lower translational kinetic energy diffuse toward higher translational energy region. The movement of gas molecules from the higher translational kinetic energy toward the lower regions is driven by advection by the moving lid (viz. Figure 7c). This is depicted in the variation of the mass transfer Peclet number in table 1; it varies from 1346 at Kn=0.001 to 20 at Kn=10.

In order to further investigate implications of the introduction of the two different flow velocities, the mass and volume velocity profiles are plotted along centerlines of the cavity for three different Knudsen numbers in Figures 7 and 8. For the low Knudsen number the two velocities profiles are identical. The clear difference is at Kn > 0.5. The volume velocity v-component in Figure 7b predicts nearly double the slip in the mass velocity. In fact, as Knudsen number increases the v-component of $\boldsymbol{U_m}$ decreases and totally vanishes in the domain at Kn=10. The volume velocity becomes dominant flow velocity in the domain in the higher Knudsen number regime as the mass velocity vanishes. This is consistent with the pressure profile in Figure 2b. For Knudsen number 10 where the mass velocity totally vanishes, the advection of molecules into the left corner and out of the right due the moving lid are represented by a positive v-component of the volume velocity on the left wall and negative component at the right Figure 7c.

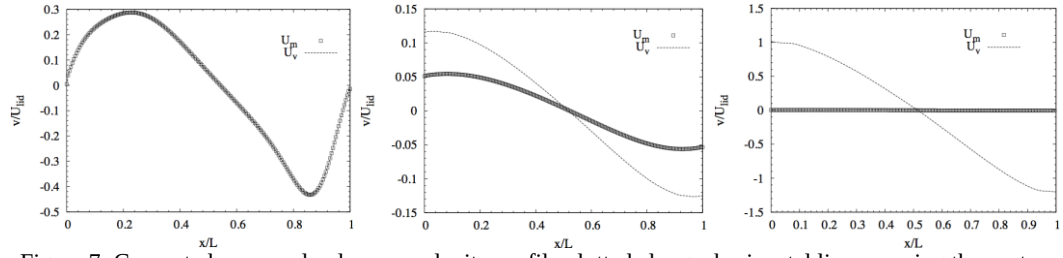

Figure 7: Computed mass and volume v-velocity profile plotted along a horizontal line, crossing the center of the cavity for (a) Kn = 0.001, (b) Kn = 0.5, (c) Kn = 10

The u-velocity profile along a vertical line crossing the cavity center is shown in Figure 8. At Kn=0.001 mass and volume velocities have the same profile and no clear slip is observed at walls. For Kn = 0.5 both methods have similar trend but differences exist in the amount of slip at walls. There is a higher u-velocity slip for the volume velocity compared to the amount of slip in the mass velocity. For Kn = 10 in Figure 8c, the normalized mass velocity is zero with no slip effects. The volume velocity shows now a reverse profile. In addition, the u-velocity slip in the volume velocity becomes large. As for the v-velocity component the volume velocity dominates the domain as the Knudsen number increases.

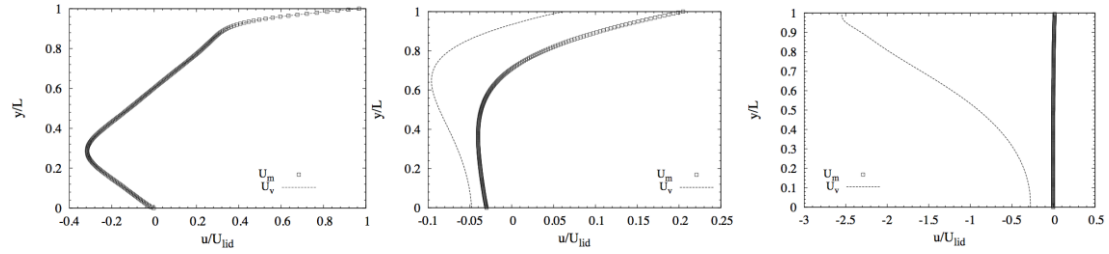

Figure 8: Computed mass and volume u-velocity profile plotted along a vertical line, crossing the center of the cavity for (a) Kn = 0.001, (b) Kn = 0.5, (c) Kn = 10

5. Conclusion

Numerical simulations have been carried out to investigate a mixed-convection problem in rarefied gas using volume diffusion continuum model. It is shown that the volume diffusion model can capture disequilibrium effects in rarefaction regime in accordance with the existing classification of the various flow regimes. Different heat transfer processes are observed for the mixed-convection problem. Volume velocity dominates the prediction of non-equilibrium effects in the upper left and right corners at high Knudsen number and affects temperature profiles across the cavity. Unconventional cold-to-hot heat transfer processes are predicted in the corners at transition regime. Future works will include the development of numerical solutions to the full four-set volume diffusion model and applications to more practical engineering flow configurations such as porous media.

References:

1. J. Koplik, and J.R. Banavar, "Corner flow in the sliding plate problem," Physics of Fluids **7**, 3118 (1995).
2. J.C. Patterson, and S. Armfield, "Transient features of natural convection in a cavity," Journal of Fluid Mechanics **219**, 469 (1990).
3. R. Iwatsu, J.M. Hyun, and K. Kuwahara, "Mixed convection in a driven cavity with a stable vertical temperature gradient," International Journal of Heat and Mass Transfer **36**, 1601 (1993).
4. B. Ghasemi, and S. Aminossadati, "Mixed convection in a lid-driven triangular enclosure filled with nanofluids," International Communications in Heat and Mass Transfer **37**, 1142 (2010).
5. T. Cheng, and W.H. Liu, "Effects of cavity inclination on mixed convection heat transfer in lid-driven cavity flows," Computers & Fluids **100**, 108 (2014).
6. C. Shen, *Rarefied gas dynamics: fundamentals, simulations and micro flows* (Springer, 2006).
7. M. Knudsen, "Die Gesetze der Molekularströmung und der inneren Reibungsströmung der Gase durch Röhren," Annalen der Physik **333**, 75 (1909).
8. S. Mizzi, D. R. Emerson, S.K. Stefanov, R.W. Barber, andJ.M. Reese, "Effects of rarefaction on cavity flow in the slip regime," Journal of computational and theoretical nanoscience **4**, 817 (2007).
9. H. Akhlaghi, E. Roohi, and S. Stefanov, "A new iterative wall heat flux specifying technique in DSMC for heating/cooling simulations of MEMS/NEMS," International Journal of Thermal Sciences **59**, 111 (2012).
10. Y. Sone, K. Aoki, S. Takata, H. Sugimoto, and A. Bobylev, "Inappropriateness of the heat-conduction equation for description of a temperature field of a stationary gas in the continuum limit: Examination by asymptotic analysis and numerical computation of the Boltzmann equation," Physics of Fluids **8**, 628 (1996).
11. H. Brenner, "Beyond Navier–Stokes," International Journal of Engineering Science **54**, 67 (2012).
12. H. Brenner, "Navier–Stokes revisited," Physica A: Statistical Mechanics and its Applications **349**, 60 (2005).
13. H. Brenner, and J. R. Bielenberg, "A continuum approach to phoretic motions: Thermophoresis," Physica A: Statistical Mechanics and its Applications **355**, 251 (2005).
14. S.K. Dadzie, "A thermo-mechanically consistent Burnett regime continuum flow equation without Chapman–Enskog expansion," Journal of Fluid Mechanics **716**, R6 (2013).
15. P. L. Walls, and B. Abedian, "Bivelocity gas dynamics of micro-channel couette flow," International Journal of Engineering Science **79**, 21 (2014).
16. S.K. Dadzie, and H. Brenner, "Predicting enhanced mass flow rates in gas microchannels using nonkinetic models," Physical Review E **86**, 036318 (2012).
17. G.A. Bird, "Definition of mean free path for real gases," Physics of Fluids **26**, 3222 (1983).

18. S.K. Dadzie, J.M. Reese, and C.R. McInnes, "A continuum model of gas flows with localized density variations," Physica A: Statistical Mechanics and its Applications **387**, 6079 (2008).
19. S.K. Dadzie, and J.M. Reese, "A volume-based hydrodynamic approach to sound wave propagation in a monatomic gas," Physics of Fluids **22**, 016103 (2010).
20. S.K. Dadzie, and J.M. Reese, "Analysis of the thermomechanical inconsistency of some extended hydrodynamic models at high Knudsen number," Physical Review E **85**, 041202 (2012).
21. M. Heida, and J. Málek, "On compressible Korteweg fluid-like materials," International Journal of Engineering Science **48**, 1313 (2010).
22. OpenCFD Ltd, *OpenFOAM*.
23. C.J. Greenshields, H.G. Weller, L. Gasparini, and J.M. Reese, "Implementation of semi-discrete, non-staggered central schemes in a colocated, polyhedral, finite volume framework, for high-speed viscous flows," International journal for numerical methods in fluids **63**, 1 (2010).
24. H. Brenner, "Fluid mechanics in fluids at rest," Physical Review E **86**, 016307 (2012).
25. C.J. Greenshields, and J.M. Reese, "The structure of shock waves as a test of Brenner's modifications to the Navier–Stokes equations," Journal of Fluid Mechanics **580**, 407 (2007).
26. M. Smoluchowski von Smolan, "Über wärmeleitung in verdünnten gasen," Annalen der Physik **300**, 101 (1898).
27. J.C. Maxwell, "On stresses in rarefied gases arising from inequalities of temperature," Proceedings of the Royal Society of London **27**, 304 (1878).